aerospace

MDPI

Article

An Improved Fault Identification Method for Electromechanical Actuators

Gaetano Quattrocchi, Pier C. Berri, Matteo D. L. Dalla Vedova * and Paolo Maggiore

Department of Aerospace and Mechanical Engineering (DIMEAS), Politecnico di Torino, 10129 Turin, Italy; gaetano.quattrocchi@polito.it (G.Q.); pier.berri@polito.it (P.C.B.); paolo.maggiore@polito.it (P.M.)
* Correspondence: matteo.dallavedova@polito.it

Abstract: Adoption of electromechanical actuation systems in aerospace is increasing, and so reliable diagnostic and prognostics schemes are required to ensure safe operations, especially in key, safety-critical systems such as primary flight controls. Furthermore, the use of prognostics methods can increase the system availability during the life cycle and thus reduce costs if implemented in a predictive maintenance framework. In this work, an improvement of an already presented algorithm will be introduced, whose scope is to predict the actual degradation state of a motor in an electromechanical actuator, also providing a temperature estimation. This objective is achieved by using a properly processed back-electromotive force signal and a simple feed-forward neural network. Good prediction of the motor health status is achieved with a small degree of inaccuracy.

Keywords: prognostics; electromechanical actuators; neural network; temperature

Citation: Quattrocchi, G.; Berri, P.C.; Dalla Vedova, M.D.L.; Maggiore, P. An Improved Fault Identification Method for Electromechanical Actuators. *Aerospace* **2022**, *9*, 341. https://doi.org/10.3390/aerospace9070341

Academic Editor: Gianpietro Di Rito

Received: 29 April 2022
Accepted: 23 June 2022
Published: 25 June 2022

1. Introduction

Electromechanical actuators (EMA) are widely used in industry, and in recent decades are seeing increasing adoption in the aviation sector, especially when the more electric or all-electric [1] design philosophies are adopted, which seeks to reduce secondary power type usage, using mostly or exclusively electrical power for systems actuation [2].

An interesting application of the more electric philosophy is in the Airbus A380 where two electrical lines are used as backup sources of power in case of loss of the main hydraulic lines. However, electrohydrostatic actuators (EHAs) are used rather than EMAs, since one of EMAs' most common failure modes is jamming [3]. Jamming is characterized by a sudden actuator stop in a certain position, thus locking the flight control surface position, creating a dangerous moments imbalance and thus possibly uncontrollable yaw, pitch or roll. Furthermore, the estimation of jamming probability is harder than for EHAs, where the knowledge regarding current hydraulic actuators can be used [4].

For this reason, as of today the use of EMAs is still mainly limited to non-safety-critical systems, such as secondary flight systems, high-lift devices or airbrakes. However, EMAs have some merits that make them preferable over other architecture, such as complexity, weight and maintenance requirements, especially in low-power applications [5]. In fact, the simplest method for providing mechanical power using an electrical supply is an electromechanical actuator, which in its most basic form is an electrical motor with a mechanism converting rotary motion to linear (using for example a ball screw). Usually, in aviation, given the high actuation torques needed and the volume constraints, some form of a reducer is incorporated between the motor and the rotation-linear converter to multiply the motor torque. A schematic view of an EMA is shown in Figure 1.

Another important aspect to consider is the lack of extensive failure datasets in operating conditions, which further discourages the adoption of EMAs given the severity of some failure modes [6]. Even though EMAs, as previously stated, are already used in secondary flight control actuation, data obtained for this use case are not directly transferable for primary flight control due to the very different operating nature of the two applications.

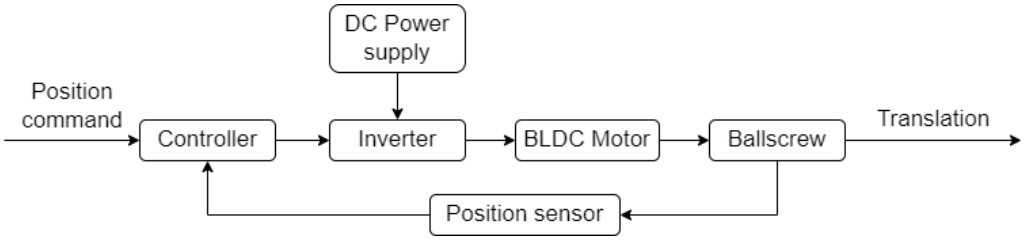

Figure 1. Block schematics of an EMA.

To increase safety and reliability, Prognostics and Health Management (PHM) could prove beneficial. The traditional definition of PHM can be found in [7], where it is defined as the ability to evaluate the current health status and predict the future behavior of a system, using knowledge of the current state; additionally, maintenance can be planned accordingly to properly maintain the system.

Several approaches to PHM exist and can be classified into three different categories: model-based, hybrid or data-driven, depending on the degree of knowledge of the system studied and the availability of data.

Model-based PHM uses a representation of the system (or component) of interest, using a set of differential Equations [8–10]. If properly modeled, the system status can be assessed with good accuracy and fault propagation is generally embedded in the fault model [11,12]. The main drawback of model-based approaches is the difficulty in creating accurate and representative models for complex systems; in particular in aeronautics, it is hard to model, or present in a simplified way, complex interactions such as aerodynamics or mechanical backlash.

The opposite approach is data-driven, where the system is treated as a black box, i.e., without detailed knowledge. In this case, machine learning methods are widely used to detect variations in the system's health status. One of the most used tools is Neural Networks of various kinds, such as in [13–16]. Some other tools used are combinations of filters and neural networks, as in [17,18], Bayesian inference [19] and Markov chains [20]. The main weakness of data-driven approaches is the need for a large dataset, which is generally not readily available, especially if run-to-failure of complex and expensive systems are needed.

Hybrid approaches use both model-based and data-driven techniques. The idea is to create a physical model of the system, extract relevant health indicators using physical quantities, and then use machine learning techniques to obtain an estimation of the actual system health status. Examples can be found in [21–24].

In this work, a hybrid prognostic method to evaluate the damage of a BLDC is presented, using the back-EMF signal as a prognostic indicator. In particular, the paper will describe an evolution of the algorithm presented in [25], which has been improved and can now also give a temperature estimate of the motor phases, besides the damage to individual stator coils and the static eccentricity of the rotor.

2. Materials and Methods

2.1. Scope of the Work and Novelties Introduced

The scope of this work is to present an evolution of the prognostic algorithm presented in [25]. The use of the back-EMF coefficient is supported by the fact that it is sensitive to the faults of interest (partial inter-turn shorts, static eccentricity), while not being affected by the command or load imposed on the actuator, as demonstrated in [26].

As previously stated, in this work the effect of temperature on phase resistance is also considered. The inclusion of temperature dependency requires a new approach to the evaluation of system status.

The algorithm can be described as follows:

1. Faults vectors are generated, and the system is simulated using these values, obtaining a simulations dataset;
2. Relevant physical quantities are logged for each simulation (e.g., voltages, currents, motor angular position and speed);
3. In each simulation, for each phase, an estimation of the back-EMF coefficient is calculated;
4. Estimation error is minimized by obtaining the real values of phase resistance and back-EMF coefficient;
5. These values are used in a neural network to predict the health status of the system.

The first two steps are self-explanatory; the faults are modeled as in [25], using a fault vector $f = [N_a,\ N_b,\ N_c,\ \xi_x,\ \xi_y,\ \Delta T]$, with 6 different components: $N_a,\ N_b,\ N_c$ which are the fraction of turns shorted for each phase; $\xi_x,\ \xi_y$ which are the components of static eccentricity in cartesian coordinates (in [25] polar coordinates are used) and finally ΔT which is the temperature deviation from reference conditions $T_0 = 20\ ^\circ$C. The variation ranges for the variables are the same as those in [25]. For stator windings temperature, the range $\Delta T = [-50;\ +70]\ ^\circ$C is chosen, since it is representative of conditions encountered in aeronautical applications. However, the range chosen might be too restrictive to include sudden transitory temperature spikes and might need adjustments in future developments. The faults are injected into the model prior to each simulation.

In the third step, the estimation of the back-EMF coefficient is obtained using the following equation:

$$V - k'\omega = V - (k + k_e)\omega = R_0 i \tag{1}$$

where k' is the estimated back-EMF coefficient and k_e is the estimation error. In this case, values of V, ω, i are those that can be measured from the simulation (and by extension, from a real system), while R_0 is the nominal resistance of a phase. There is an error in the estimation of the back-EMF coefficient since the nominal resistance is used, thus not considering the effect of both a temperature variation and partial phase to phase short, which changes this value.

The actual (or true) system condition is described by:

$$V - k\omega = R \cdot i = (R_0 + \Delta R)i \tag{2}$$

where k is the true back-EMF coefficient, $R = (R_0 + \Delta R)$ is the true resistance, i.e., the effective resistance of the coil in the instantaneous conditions of temperature, fault, etc. and ΔR is the deviation of actual resistance from nominal value.

Now, subtracting Equation (2) from Equation (1) and rearranging, one can obtain:

$$k_e = \Delta R \frac{i}{\omega} \tag{3}$$

Assuming that ΔR is constant (i.e., R varies slowly), which is reasonable in the framework presented, since each measurement is very short (in the order of one second), derivating Equation (3) we have:

$$\frac{\partial k_e}{\partial (i/\omega)} = \Delta R \tag{4}$$

Furthermore, assuming that k is constant, which implies that the fault does not change during the simulation, we can obtain:

$$\frac{\partial (k + k_e)}{\partial (i/\omega)} = \frac{\partial k'}{\partial (i/\omega)} = \Delta R \tag{5}$$

So, we have demonstrated that $k' = (k + k_e)$ is linearly dependent to i/ω with a slope equal to ΔR. Now, to obtain the real values of back-EMF coefficient and resistance, we have to iteratively reconstruct the value of k (Equation (2)), using a temporary R^* variable to optimize to make Equation (5) equal to zero. This stems from the definition of back-EMF:

$$|BEMF| = \frac{\partial \Phi}{\partial t} = \frac{\partial \Phi}{\partial \theta}\frac{\partial \theta}{\partial t} = \frac{\partial \Phi}{\partial \theta}\omega \quad \rightarrow \quad k_j(n_j, \theta, T) = \frac{\partial \Phi(n_j, \theta, T)}{\partial \theta} \tag{6}$$

where Φ is the concatenated magnetic flux, n is the number of shorted turns and T is the temperature. In other words, the concatenated magnetic flux is a function of angle, number of turns and temperature and so is the back-EMF coefficient k_j. It does depend only on motor geometry and on the magnetic properties of the magnets, and thus the temperature dependency. In this preliminary work, the temperature-induced variation of magnetic properties is not considered and will be added in further developments.

The following problem must then be solved:

$$\begin{cases} V - k^*\omega = R^* \cdot i \\ \dfrac{\partial(k^*)}{\partial(i/\omega)} = 0 \end{cases} \tag{7}$$

At convergence, we obtain $R^* = R$ which implies $k_e = 0$ (from Equation (2)): we are calculating true resistance and true back-EMF coefficient. In this work, a simple bisection method is used to perform the optimization.

Up to this point, we have considered $k_j(\theta,\ i/\omega)$, as visible in Figure 2, where the subscript j indicates one of the three phases; in this case, the number of variables to optimize will be $3 \cdot n$, where n is the number of subdivisions along the θ axis. The total number of variables will thus be $6 \cdot n$, i.e., $3n$ values of resistance and $3n$ values of back-EMF coefficient.

However, in order to simplify the computation, the dependence on θ has been dropped, thus collapsing the 3D graph into a 2D plot of $k_j(i/\omega)$, i.e., Figure 3. Now, a 'global' (or *generalized*) k_j approximation can be calculated, using least square fit. Values close to zero have been discarded, since they provide no additional information, and an absolute value on k_j has been applied. The final result is a reduction of the number of variables from $6 \cdot n$ to 6, i.e., 3 generalized resistances (one for each phase) and 3 generalized back-EMF coefficients.

These 6 values are used in a simple feed-forward neural network to perform an estimation of the fault vector f.

Figures 2 and 3 have been obtained using a parabolic position command (i.e., a speed ramp) with a constant angular acceleration of 0.3 rad/s^2; initial conditions are zero angular position and zero angular velocity ($\theta = \dot{\theta} = 0$). The following fault vector was seeded: $f = [0.0375,\ 0.0504,\ 0.0507,\ 0.0059,\ 2.8 \times 10^{-5},\ 4]$.

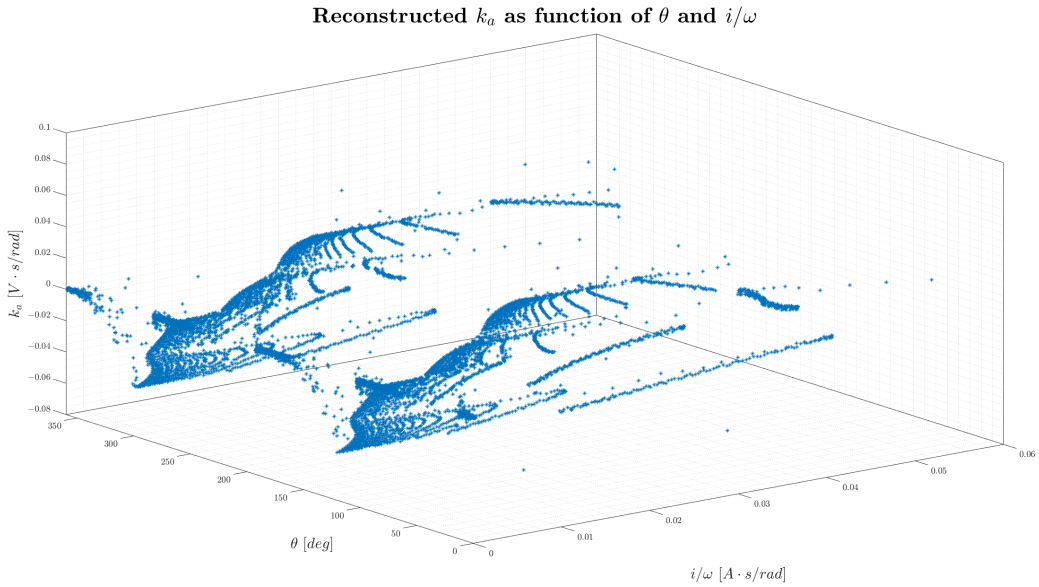

Figure 2. Reconstructed k_a as function of both θ and i/ω.

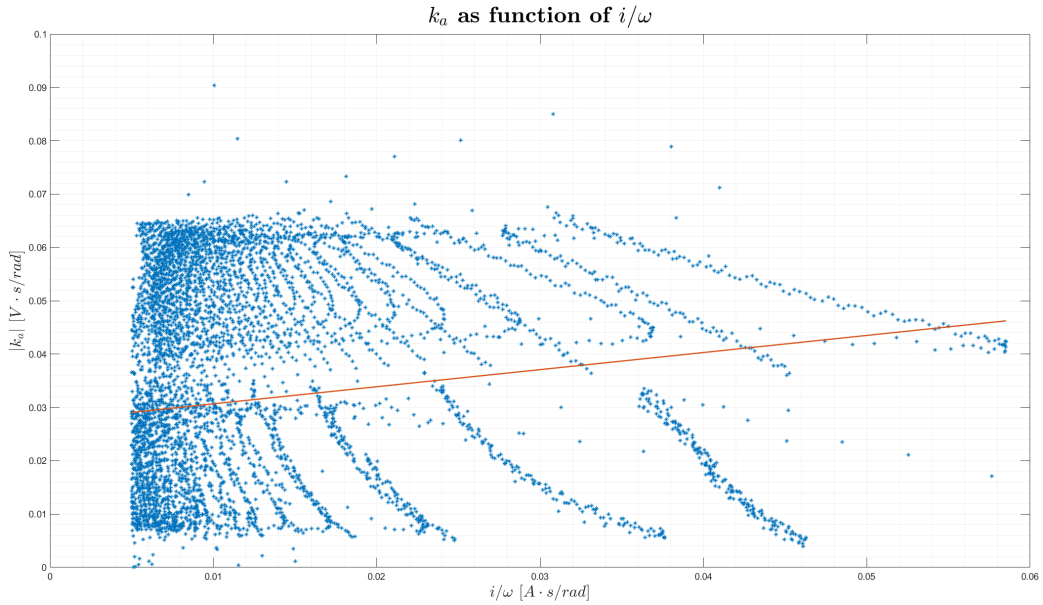

Figure 3. Reconstructed k_a as function of i/ω (non optimized).

2.2. Brief System Overview

As previously stated, the system used to test the algorithm is the same as that used in [25,26], with minor modifications (Figure 4); it represents an electromechanical actuator acting on a flight surface.

The model is a high fidelity representation of a trapezoidal EMA acting on secondary flight control. It is a detailed, component-level model with very limited assumptions, i.e., lumped parameters. Many non-linear phenomena are modeled, including but not limited to electronic noise, dry friction and current and speed saturations. The model has been validated on literature data as reported in [27,28]. For further details on the model, please refer to [26].

With respect to previous iterations, the main enhancement is the implementation of a temperature dependency on phase resistance (each of the three RL branches in Figure 5), using the classical equation:

$$R = R_{ref}(1 + \alpha \Delta T) \tag{8}$$

where $\alpha = 0.00404\ ^{\circ}\mathrm{C}^{-1}$ is the resistance temperature coefficient of copper (the materials of which the coils are made), R_{ref} is the reference temperature resistance (in this case $T_{ref} = 20\ ^{\circ}\mathrm{C}$) and ΔT is the temperature difference from T_{ref}.

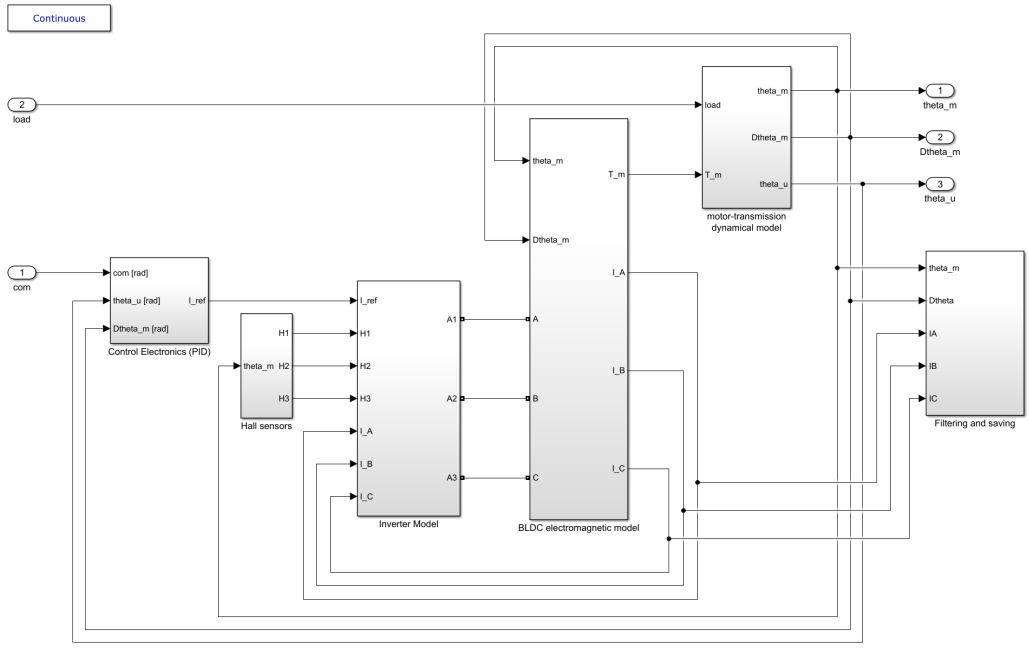

Figure 4. Top level view of the actuator model.

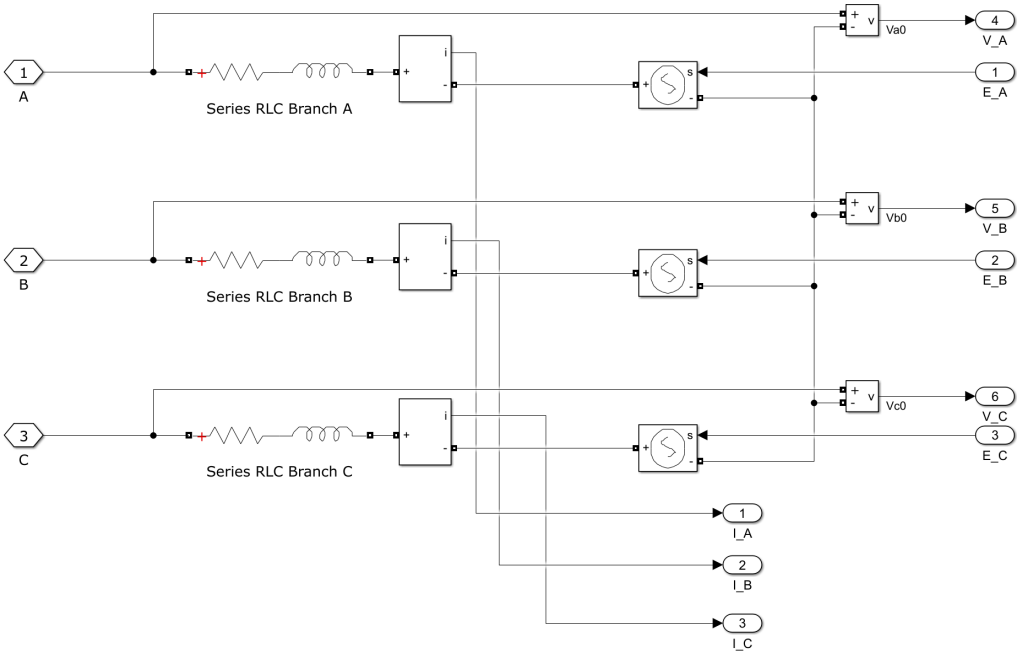

Figure 5. Phases model detail (a subsystem of 'BLDC electromagnetic model').

Furthermore, the external load is set to zero, supposing an actuation during ground operations, while the actuation command is now a parabolic position command (i.e., a velocity ramp, or constant acceleration), since using this type of command better covers the (i/ω) space and thus embed more information in the same simulation time as opposed to more classical commands such as position ramps or steps.

Some examples of the data obtained after simulations can be found in Figures 6 and 7. It can be noted how the first ∼40 ms present strong fluctuations in the current and voltages

values (but also angular velocity): this is due to the strong non-linear effects modeled in the system, e.g., dry friction. For this reason, the first ∼50 ms of each simulation are discarded before applying the algorithm presented.

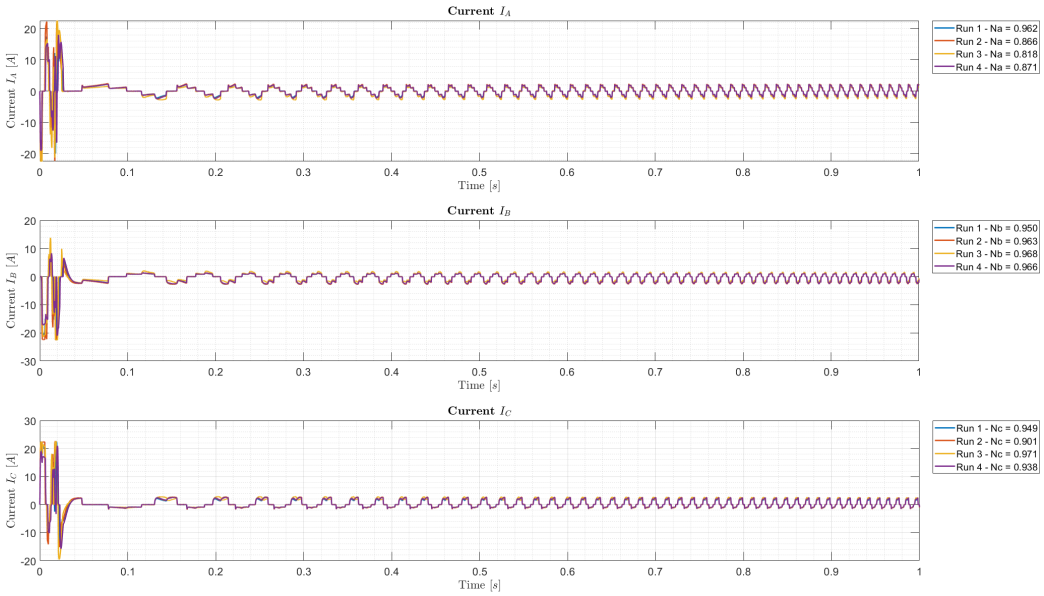

Figure 6. Graphs of phase current for different fault conditions.

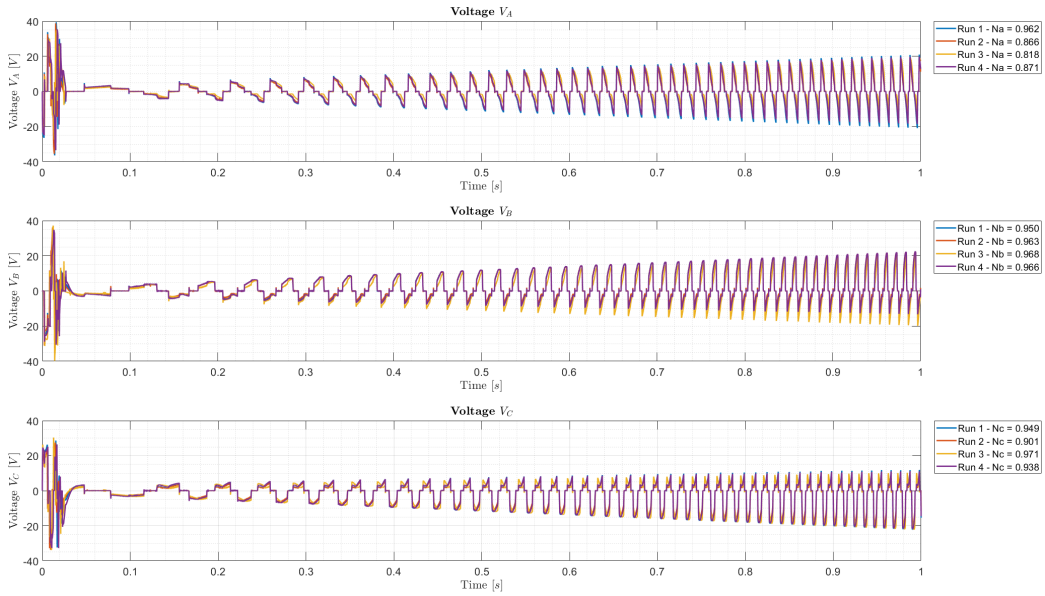

Figure 7. Graphs of phase voltage for different fault conditions.

2.3. Dataset Used

The number of different fault conditions simulated is 600; the dataset has been randomly divided into 70%, 15%, 15% subsets for training, validation and testing, respectively.

Dataset size has been empirically chosen to be a good representation of the 6-dimensional fault space; the dataset, regarding the first 5 variables of the fault vector (N_a, N_b, N_c, ξ_x, ξ_y) is the same presented in [25], with the two eccentricity components now transformed into cartesian coordinates from polar. For each fault vector, a temperature difference value (ΔT), randomly sampled from the interval considered, has been appended.

Using an AMD 5600X, each simulation takes about 50 s to run; parallel pooling has been used to reduce the total dataset generation time, combined with Simulink Accelerator mode. For this study, a full software workflow has been used. In other words, the full

system is simulated and relevant data logged. The algorithm presented is then applied and neural network outputs are compared to the fault vectors injected in the model before simulation, which are considered ground truth.

In the future, we hope to implement the faults considered in this study on a real test bench, even though it is a complex task, especially for the partial phase shorts.

3. Results

In this section, the network used for fault regression will be described. Several tests on different hyperparameter combinations have been carried out, and the best performing set has been used for error distribution calculation. The network architecture is very similar to that presented in [25], with minor modifications to the values of the hyperparameters.

The architecture chosen is a feed-forward neural network with a single hidden layer of size 12 (Figure 8); the training function uses the Levenberg–Marquardt algorithm; the activation function for each neuron is the hyperbolic tangent sigmoid. The maximum size of failed validation checks is set to 10.

As expected, the network inputs vector is of size 6—including 3 generalized back-EMF coefficients and 3 generalized resistances, while the output is again of size 6 and is the fault vector used to generate the simulation.

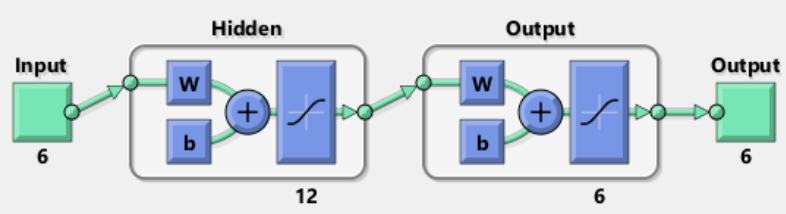

Figure 8. Neural network topology.

In Figure 9, the mean absolute error box plot for each variable is shown. For visualization purposes, a new subset of 10 rows is used and called an external validation set. This dataset has never been used during training of the neural network so it is a good representation of the predictive capabilities of the network with new data during operations. As visible, the mean absolute error is very small, in the order of 0.02 on normalized data. The error distribution is however uneven between variables and this might be caused by the relatively small dataset used in training.

In absolute terms, the mean error for the ΔT estimation, on the external verification dataset, is about 1.8 °C, which is a good result.

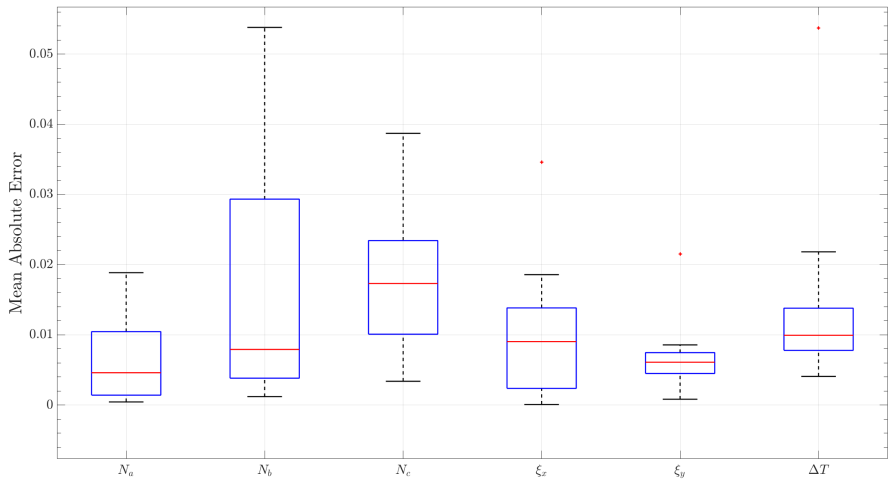

Figure 9. Mean absolute error for external validation set.

4. Discussion

As described in the previous section, the prediction accuracy of the system is promising. Even though the problem complexity has increased with respect to the previous algorithm [25], the neural network is capable of predicting the system status with adequate accuracy.

The network regression task is probably aided by the extensive pre-processing applied to raw data before being used as an input dataset, including filtering. In a real system, properly calibrated filtering will be needed to smooth out high-frequency noise in the signals of interest, before the application of the algorithm is presented.

Furthermore, the data compression techniques described in Section 2.1 are helpful in reducing the dimensions of the regression problem, even though the estimation obtained is a generalization of the health status rather than an estimation for each possible angular position.

5. Conclusions

In this work, an improved prognostic algorithm for EMA has been presented. The strong points of this paper include the ability to estimate the current health status of the motor in terms of fault variables including partial phase shorts, static eccentricity and temperature deviation from ambient conditions. Furthermore, no additional sensors besides those needed for normal operations are required. Motor damage estimation is carried out using a feed-forward neural network after the application of the algorithm to raw data.

As with any other work that includes neural networks in the pipeline, a parametric optimization of the network could yield additional benefits in the form of higher accuracy or a simpler network if the algorithm is to be implemented on embedded hardware.

Furthermore, several assumptions have been made to simplify the algorithm, mainly the temperature independence of magnetic properties. Even though it is a reasonable assumption for small variations of temperature (magnetic flux variation of ca. -4% for 100 °C for SaCo magnets), a generalized algorithm should include and simulate such variations.

An increase in the simulation dataset size, after considering what the best combination of actuation command and load is, could prove beneficial in further increasing the network accuracy and robustness.

Finally, an empirical validation on properly calibrated equipment is mandatory to test that the assumptions made are reasonable and can effectively represent the system status.

Author Contributions: Conceptualization, P.C.B.; methodology, G.Q. and P.C.B.; software, G.Q.; validation, G.Q.; formal analysis, G.Q. and P.C.B.; investigation, G.Q.; resources, G.Q.; data curation, G.Q.; writing—original draft preparation, G.Q.; writing—review and editing, G.Q. and M.D.L.D.V. visualization, G.Q.; supervision, M.D.L.D.V. and P.M.; project administration, M.D.L.D.V. and P.M.; funding acquisition, M.D.L.D.V. and P.M. All authors have read and agreed to the published version of the manuscript.

Funding: This research received no external funding.

Informed Consent Statement: Not applicable.

Data Availability Statement: The datasets needed to replicate what was presented in this study are openly available in FigShare at doi:10.6084/m9.figshare.19635378, accessed on 24 June 2022.

Conflicts of Interest: The authors declare no conflict of interest.

Abbreviations

The following abbreviations are used in this manuscript:

BEMF	Back Electro-Motive Force;
BLDC	BrushLess Direct Current;
EHA	Electrohydrostatic Actuator;
EMA	Electro-Mechanical Actuator;
FDI	Fault Detection and Identification;
PHM	Prognostics and Health Management.

References

1. Quigley, R.E.J. More Electric Aircraft. In Proceedings of the Eighth Annual Applied Power Electronics Conference and Exposition, Long Beach, CA, USA, 17–21 March 2013; pp. 906–911. [CrossRef]
2. Wheeler, P.; Bozhko, S. The more electric aircraft: Technology and challenges. *IEEE Electrif. Mag.* **2014**, *2*, 6–12. [CrossRef]
3. Balaban, E.; Bansal, P.; Stoelting, P.; Saxena, A.; Goebel, K.F.; Curran, S. A diagnostic approach for electro-mechanical actuators in aerospace systems. In Proceedings of the 2009 IEEE Aerospace Conference, Big Sky, MT, USA, 7–14 March 2009; pp. 1–13.
4. Van Den Bossche, D. The A380 flight control electrohydrostatic actuators, achievements and lessons learnt. In Proceedings of the 25th International Congress of the Aeronautical Sciences, Hamburg, Germany, 3–8 September 2006; International Council of Aeronautical Sciences (ICAS): Hamburg, Germany, 2006; pp. 1–8.
5. Botten, S.L.; Whitley, C.R.; King, A.D. Flight control actuation technology for next-generation all-electric aircraft. *Technol. Rev. J.* **2000**, *8*, 55–68.
6. Hussain, Y.M.; Burrow, S.; Henson, L.; Keogh, P. A review of techniques to mitigate jamming in electromechanical actuators for safety critical applications. *Int. J. Progn. Health Manag.* **2018**, *9*, 1–11. [CrossRef]
7. Vachtsevanos, G.J.; Vachtsevanos, G.J. *Intelligent Fault Diagnosis and Prognosis for Engineering Systems*; Wiley: Hoboken, NJ, USA, 2006; Volume 456.
8. Tinga, T.; Loendersloot, R. Physical model-based prognostics and health monitoring to enable predictive maintenance. In *Predictive Maintenance in Dynamic Systems*; Springer: Berlin/Heidelberg, Germany, 2019; pp. 313–353.
9. Yiwei, W.; Christian, G.; Binaud, N.; Christian, B.; Jian, F. A model-based prognostics method for fatigue crack growth in fuselage panels. *Chin. J. Aeronaut.* **2019**, *32*, 396–408.
10. Di Rito, G.; Luciano, B.; Borgarelli, N.; Nardeschi, M. Model-Based Condition-Monitoring and Jamming-Tolerant Control of an Electro-Mechanical Flight Actuator with Differential Ball Screws. *Actuators* **2021**, *10*, 230. [CrossRef]
11. Ray, A.; Tangirala, S. A nonlinear stochastic model of fatigue crack dynamics. *Probabilistic Eng. Mech.* **1997**, *12*, 33–40. [CrossRef]
12. Swindeman, R.; Swindeman, M. A comparison of creep models for nickel base alloys for advanced energy systems. *Int. J. Press. Vessel. Pip.* **2008**, *85*, 72–79. [CrossRef]
13. Li, X.; Ding, Q.; Sun, J.Q. Remaining useful life estimation in prognostics using deep convolution neural networks. *Reliab. Eng. Syst. Saf.* **2018**, *172*, 1–11. [CrossRef]
14. Guo, L.; Li, N.; Jia, F.; Lei, Y.; Lin, J. A recurrent neural network based health indicator for remaining useful life prediction of bearings. *Neurocomputing* **2017**, *240*, 98–109. [CrossRef]
15. Xia, M.; Zheng, X.; Imran, M.; Shoaib, M. Data-driven prognosis method using hybrid deep recurrent neural network. *Appl. Soft Comput.* **2020**, *93*, 106351. [CrossRef]
16. Al-Dulaimi, A.; Zabihi, S.; Asif, A.; Mohammadi, A. A multimodal and hybrid deep neural network model for Remaining Useful Life estimation. *Comput. Ind.* **2019**, *108*, 186–196. [CrossRef]
17. Liu, J.; Zhang, M.; Zuo, H.; Xie, J. Remaining useful life prognostics for aeroengine based on superstatistics and information fusion. *Chin. J. Aeronaut.* **2014**, *27*, 1086–1096. [CrossRef]
18. Baptista, M.; Henriques, E.M.; de Medeiros, I.P.; Malere, J.P.; Nascimento, C.L., Jr.; Prendinger, H. Remaining useful life estimation in aeronautics: Combining data-driven and Kalman filtering. *Reliab. Eng. Syst. Saf.* **2019**, *184*, 228–239. [CrossRef]
19. Jianzhong, S.; Fangyuan, W.; Shungang, N. Aircraft air conditioning system health state estimation and prediction for predictive maintenance. *Chin. J. Aeronaut.* **2020**, *33*, 947–955.
20. Li, Q.; Gao, Z.; Tang, D.; Li, B. Remaining useful life estimation for deteriorating systems with time-varying operational conditions and condition-specific failure zones. *Chin. J. Aeronaut.* **2016**, *29*, 662–674. [CrossRef]
21. Liu, J.; Wang, W.; Ma, F.; Yang, Y.; Yang, C. A data-model-fusion prognostic framework for dynamic system state forecasting. *Eng. Appl. Artif. Intell.* **2012**, *25*, 814–823. [CrossRef]
22. Wang, B.; Lei, Y.; Li, N.; Li, N. A hybrid prognostics approach for estimating remaining useful life of rolling element bearings. *IEEE Trans. Reliab.* **2018**, *69*, 401–412. [CrossRef]
23. Wang, P.; Long, Z.; Wang, G. A hybrid prognostics approach for estimating remaining useful life of wind turbine bearings. *Energy Rep.* **2020**, *6*, 173–182. [CrossRef]
24. Quattrocchi, G.; Iacono, A.; Berri, P.C.; Dalla Vedova, M.D.; Maggiore, P. A New Method for Friction Estimation in EMA Transmissions. *Actuators* **2021**, *10*, 194. [CrossRef]

25. Quattrocchi, G.; Berri, P.C.; Dalla Vedova, M.D.L.; Maggiore, P. Innovative Actuator Fault Identification Based on Back Electromotive Force Reconstruction. *Actuators* **2020**, *9*, 50. [CrossRef]
26. Berri, P.C.; Dalla Vedova, M.; Maggiore, P. A Lumped Parameter High Fidelity EMA Model for Model-Based Prognostics. In Proceedings of the 29th ESREL, Hannover, Germany, 22–26 September 2019; pp. 22–26.
27. Belmonte, D.; Dalla Vedova, M.; Maggiore, P. Electromechanical servomechanisms affected by motor static eccentricity: Proposal of fault evaluation algorithm based on spectral analysis techniques. In *Safety and Reliability of Complex Engineered Systems, Proceedings of the 25th European Safety and Reliability Conference, ESREL 2015, Zürich, Switzerland, 7–10 September 2015*; CRC Press: London, UK, 2015; pp. 2365–2372.
28. Belmonte, D.; Dalla Vedova, M.; Maggiore, P. Prognostics of Onboard Electromechanical Actuators: A New Approach Based on Spectral Analysis Techniques. *Int. Rev. Aerosp. Eng.* **2018**, *11*, 96–103. [CrossRef]